JMEPEG (1997) 6:240-246

Inverse Resolution of the Heat-Transfer Equation with Internal Heat Source: Application to the Quenching of Steels with Phase Transformations

P. Archambault, S. Denis, and A. Azim

A method is described for calculating the time dependence of the temperature and heat flux (on heating and cooling) at the surface of a solid body. For a given ambient temperature and a known time-temperature function of an interior point, the surface heat flux is computed through an inverse conduction algorithm taking into account the nonlinear nature of the problem. Moreover, this algorithm includes the enthalpy of phase transformations. The influence of space and time steps on inverse calculations (precision, stability) is investigated. The method is then applied to thermal cases involving different transformations in steels.

Keywords
heat conduction transfer, inverse conduction algorithm, phase transformation

1. Introduction

GENERALLY, heat treating of metallic mechanical parts involves different temperature-dependent phenomena, such as thermal gradients, deformations, stresses, and metallurgical transformations. These processes affect the final state of the treated part (e.g., structure, mechanical properties, residual stresses, and surface hardening), but can be strongly interdependent through complex relationships. In order to simulate the entire heat treatment, one must take into account this interdependence with the aid of specific, but connected, algorithms.

The basis of these phenomena is the thermal evolution of the part, which must be precisely controlled to reach the desired properties. However, if one can easily measure the temperature of inner locations, the time dependence of the thermal flux at the surface of the part is not experimentally accessible and must be calculated for further thermal, mechanical, and metallurgical calculations.

Prediction of thermal distribution and surface heat flux involves an inverse heat conduction calculation, which has already been treated by many investigators. Unlike analytical methods, which are limited to linear one-dimensional problems, discrete methods based on finite differences or finite elements can be applied to any problem (Ref 1-4). However, these latter methods induce numerical noise and oscillations due to the unstable nature of the inverse problem.

In addition, previous investigations considered pure thermal problems with no internal source of energy. This must be reconsidered in the case of materials such as steels which present endothermal or exothermal metallurgical transformations during heat treating. The aim of the present study is the association of thermal and metallurgical processes in a global heat conduction inverse resolution algorithm.

This paper describes the different components of the model and its numerical validation. The model is then applied to heat treatment of steels.

P. Archambault and **S. Denis,** Laboratoire de Science et Génie des Matériaux Métalliques (LSG2M, URA CNRS 159), École des Mines, Parc de Saurupt, 54042 Nancy, France; and **A. Azim,** Université Chouaib Doukkali, Faculté des Sciences, Département de Physique, BP 20, El-Jadida, Morocco.

2. Problem Formulation

Let us consider a one-dimensional heat conduction problem applied to an infinite cylinder initially at uniform temperature T_0. Our aim is to calculate the heat flux at the surface of the cylinder, given the temperature evolution measured at inner location $r = r_e$ and considering the internal energy source.

The heat conduction transfer is then governed by:

$$\rho C_p \frac{\partial T}{\partial t} = \frac{1}{r}\frac{\partial}{\partial r}\left(r \lambda \frac{\partial T}{\partial r}\right) + \dot{Q}(r,t)$$

where λ is thermal conductivity, C_p is specific heat, ρ is density, and $\dot{Q}$ is the internal energy generated by phase transformations. The initial and boundary conditions are:

$t = 0$

$T(r,0) = T_0$

$\dot{Q}(r,0) = 0$

$t > 0$

$$\left(\frac{\partial T}{\partial r}\right)_{r=0} = 0$$

$$-\lambda\left(\frac{\partial T}{\partial r}\right)_{r=R} = \phi \text{ (to be estimated)}$$

$T(r_e,t) = r(t)$ (measured)

$\dot{Q}(r,t)$ (calculated, metallurgy dependent)

where R is the radius of the cylinder ($r_e < R$) and ϕ is the surface heat flux.

2.1 *Inverse Heat Conduction Method*

In this study, we have adapted the inverse method already developed (Ref 5) in order to take into account the phase transformations that can arise during heat treatment of the considered alloy. This method requires solving two separate problems (Fig. 1).

The *direct conduction problem* involves calculating at each time step the temperature profile in the inner region ($0 \le r \le r_e$) for which all the boundary conditions are known. The numerical method employed here is a classical implicit standard finite-difference algorithm.

Inverse conduction problem. With the previously calculated temperature field in the direct region and the measured temperature history at location r_e, an inverse space marching finite-difference algorithm is then used to determine the temperature field in the inverse region ($r_e < r < R$).

The temperature distribution in the inverse region (i = e to i = M – 1) is obtained by:

$$T_{i+1}^j = \frac{1}{C_i^j}\left[T_i^{j-1} + D_i^j \dot{Q}_i^j - A_i^j T_{i-1}^j - B_i^j T_i^j\right]$$

with

$$A_i^j = -\left[\frac{\Delta t}{(\Delta r_2)^2}\left(1 - \frac{\Delta r_2}{2r_i}\right)\frac{\lambda_{i+1/2}^j}{(\rho C_p)_i^j}\right]$$

$$C_i^j = -\left[\frac{\Delta t}{(\Delta r_2)^2}\left(1 + \frac{\Delta r_2}{2r_i}\right)\frac{\lambda_{i+1/2}^j}{(\rho C_p)_i^j}\right]$$

$$B_i^j = 1 + A_i^j + C_i^j$$

$$D_i^j = \frac{\Delta t}{(\rho C_p)_i^j}$$

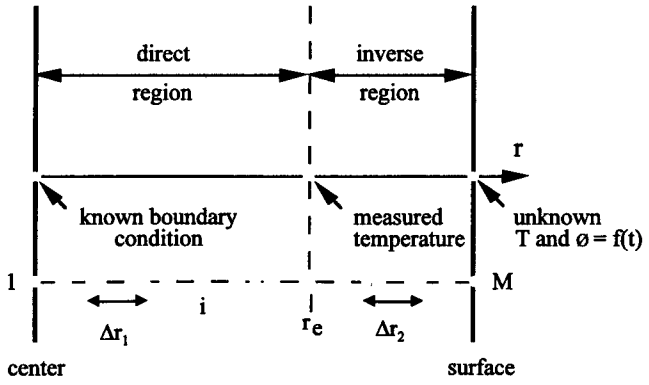

Fig. 1 Illustration of the inverse problem (direct and inverse regions)

where i and j stand for space and time incrementation, respectively.

At the end, the unknown surface heat flux is calculated from the energy balance at the surface node M. It is given by:

$$\phi_M^j = -\rho\, C_p\, T_M^j \frac{T_M^{j+1} - T_M^{j-1}}{2\Delta t}\Delta r_2 - \left(1 - \frac{1}{M-1}\right)\lambda\, T_{M-1}^j \frac{T_M^j - T_{M-1}^j}{\Delta r_2} - \dot{Q}_M^j \Delta r_2$$

2.2 *Phase Transformation Calculation*

The basis of the phase transformation modeling has been developed and applied to steels previously (Ref 6). The heat involved during a phase transformation is related to the kinetics of the different activated transformations through:

$$\dot{Q} = \sum_k \Delta H_k \frac{dy_k}{dt}$$

where ΔH_k is the transformation enthalpy and y_k is the volume fraction of constituent k. This term assures the thermal-phase transformation coupling.

The thermophysical properties (λ, ρ, C_p) depend on temperature and on the volume fractions of transformed phases through a linear mixture rule, as exemplified below for thermal conductivity (n components):

$$\lambda = \sum_{k=1}^{n} y_k(r,t)\, \lambda_k\left[T(r,t)\right]$$

The phase transformation calculation is based on the additivity principle. The continuous temperature-time evolution is discretized in a series of isothermal steps. At each step, the volume fraction of each phase is calculated. For diffusion-controlled transformations, the incubation process is first treated according to Scheil's method:

$$S = \sum_i \frac{\Delta t_i}{\tau(T_i)}$$

where Δt_i is the time step and $\tau(T_i)$ is the incubation time of the isothermal transformation at temperature T_i. When $S = 1$, the growth process is involved by using isothermal transformation kinetics, which are modeled according to Johnson-Mehl-Avrami's law; that is, for constituent k at a given temperature:

$$y_k = y_{max\,k}\left[1 - \exp\left(-b_k t^{n_k}\right)\right]$$

where y_k is the volume fraction transformed at time t and $y_{max\,k}$ is the maximum volume fraction of constituent k that can be formed at that temperature. The coefficients b_k and n_k are cal-

culated with the aid of experimental isothermal transformation (IT) kinetics obtained for a set of temperatures.

The diffusionless transformation (i.e., martensitic transformation) is calculated using Koïstinen and Marburger's relation:

$$y_k = 1 - \exp\,[-A_m(M_s - T)]$$

where A_m is the Koïstinen and Marburger coefficient and M_s is the martensitic transformation start temperature. A further description of the metallurgical parameters included in this phase transformation model can be found in Ref 6.

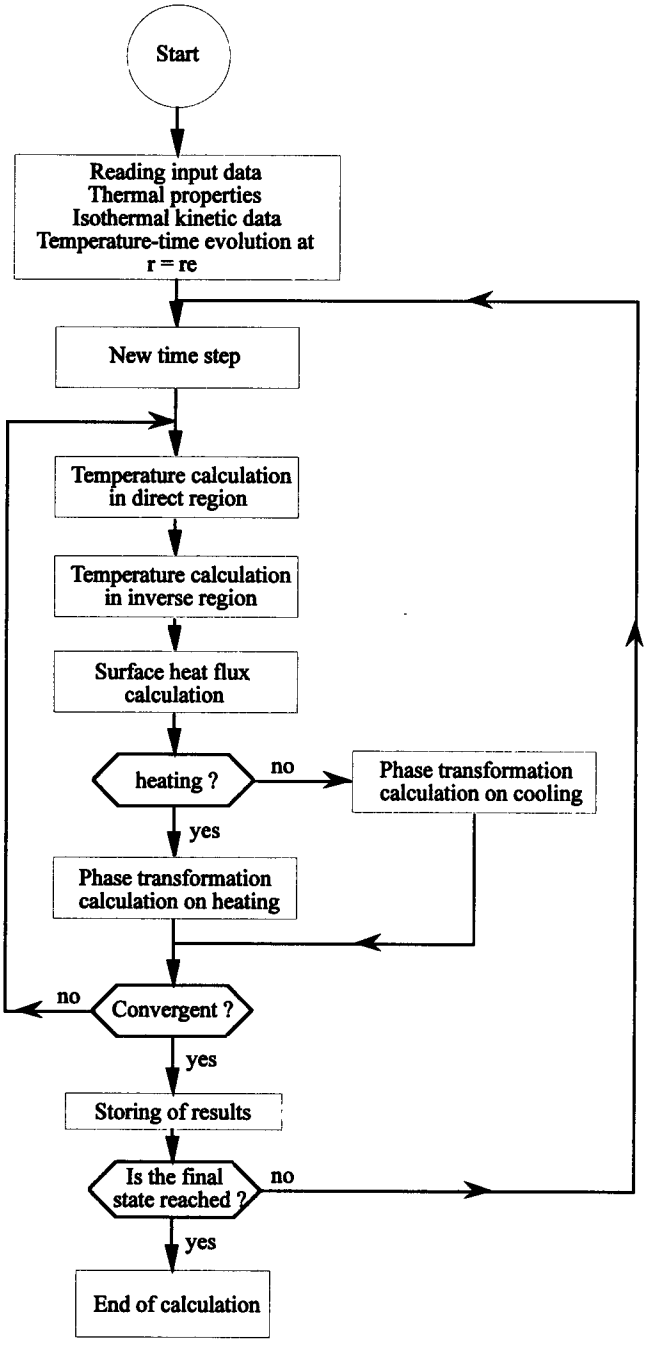

Fig. 2 Simplified flowchart of the entire procedure

A simplified flowchart of the numerical calculation developed for coupling the thermal inverse method and phase transformation model is shown in Fig. 2. For metallurgical considerations, the phase transformation modeling is divided in two parts for heating and cooling thermal evolutions. The main results obtained at the end of the calculation are:

- Temperature distribution along the radius
- Surface heat flux density evolution
- Phase volume fractions variations with time
- Phase volume fractions along the radius
- Radial hardness profile

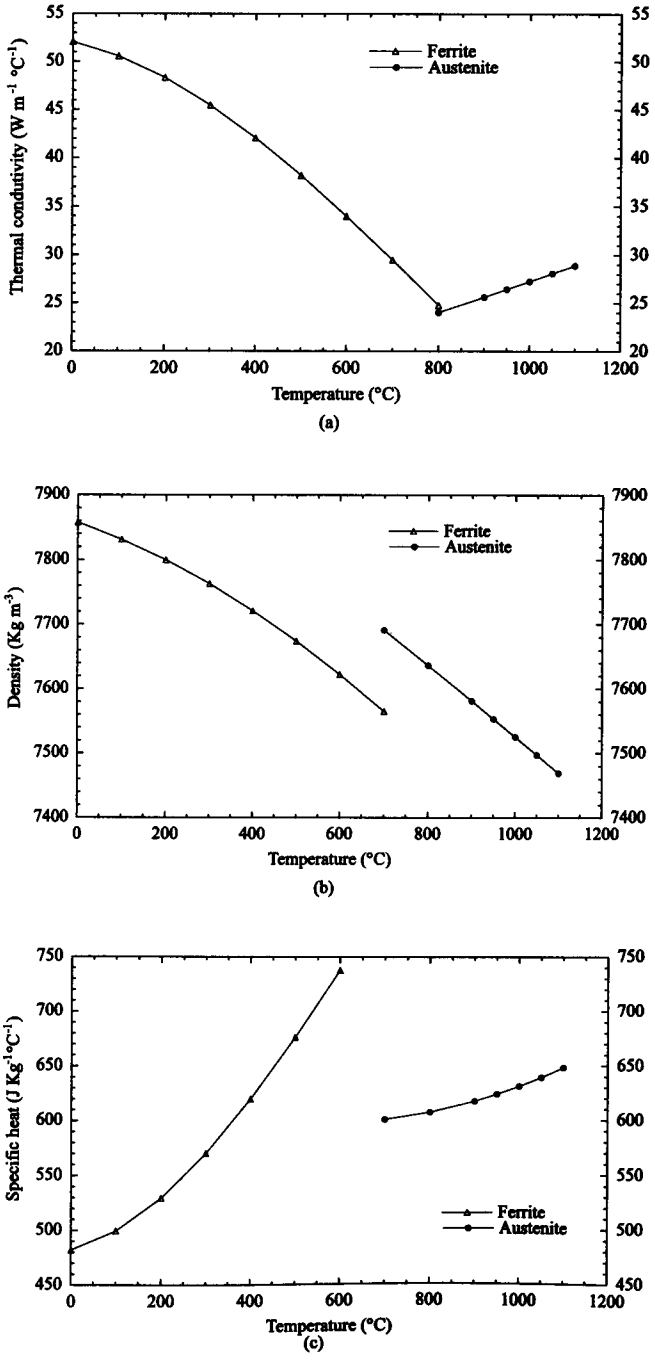

Fig. 3 Thermophysical properties of the XC42 steel

3. Tests and Results

The response of the method has been tested on cylindrical specimens (ϕ = 16 mm) for hypoeutectoid (XC42) and eutectoid (XC80) carbon steels presenting different phase transformations on heating and cooling (austenitic, martensitic, and pearlitic transformations).

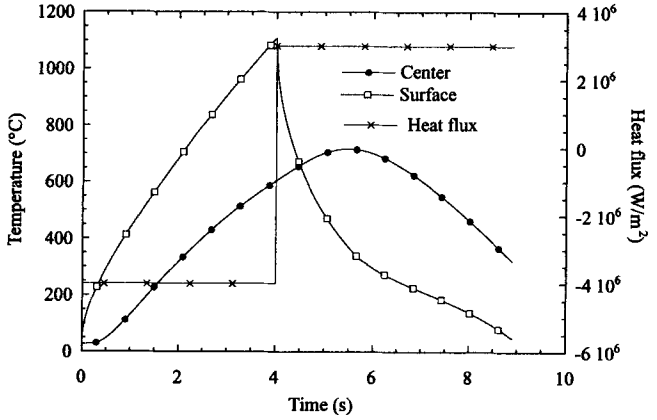

Fig. 4 Direct calculation: input exact heat flux and calculated temperature evolutions

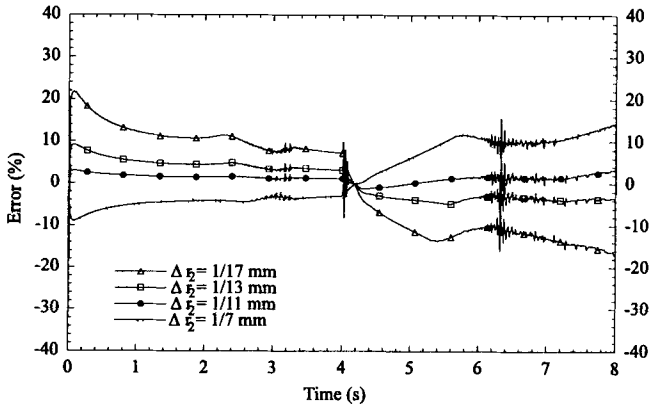

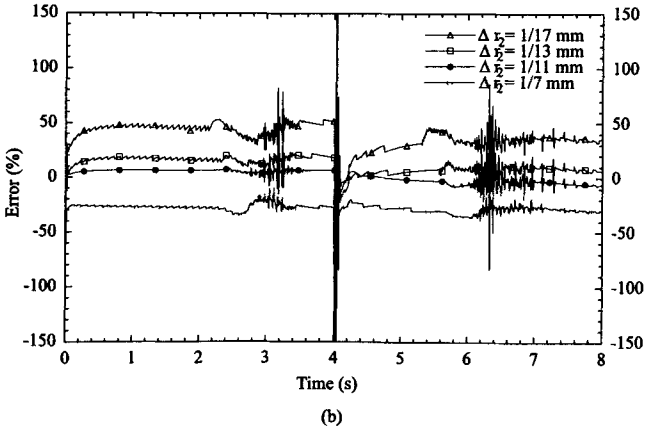

Fig. 5 Influence of space step Δr_2 for Δt = 0.01 s. Results at $r = R$: (a) temperature deviation; (b) heat flux deviation

3.1 *Calculation Input Data*

For the alloys under consideration, the main thermal input data are the variations of the thermophysical properties with temperature for each constituent and the transformation enthalpy for each phase transformation. Figure 3 shows the thermophysical properties of austenite and ferrite versus temperature for the XC42 steel (Ref 7).

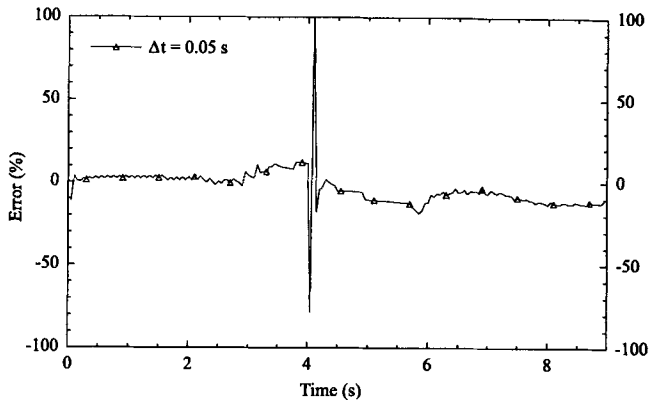

(a)

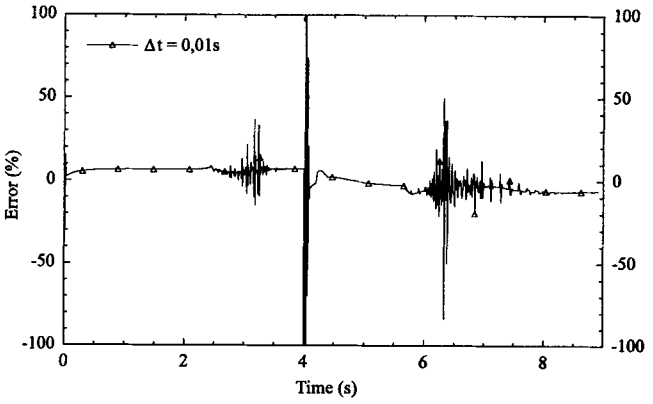

(b)

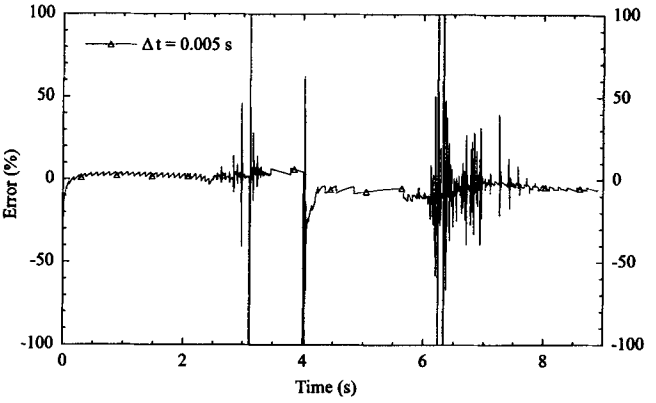

(c)

Fig. 6 Influence of time step for Δr_2 = 1/11 mm: heat flux error

The transformation enthalpy values for XC42 and XC80 are given by:

- XC42

$\Delta H = -3.05 \times 10^8 + 9.26 \times 10^3 T + 9.91T^2$ (J/m^3) (pearlite-ferrite → austenite)

$\Delta H = 6.48 \times 10^8$ J/m^3 (martensite transformation)

- XC80

$\Delta H = -1.56 \times 10^9 + 1.50 \times 10^6 T$ (ΔH, J/m^3; T, °C) (pearlite → austenite)

$\Delta H = 1.56 \times 10^9 - 1.50 \times 10^6 T$ (ΔH, J/m^3; T, °C) (austenite → pearlite)

The data used in the phase transformation calculation are IT curves on heating and IT curves for the onset of transformation, for 10% and 90% constituent formed during the cooling (Ref 6, 8).

3.2 *Influence of Space and Time Steps*

First, the numerical solution of the direct conduction problem for a given heat flux evolution imposed at the surface of the cylinder is used to generate the temperature evolution at inner position $r = r_e$ (1 mm under the active surface). This set point and the calculated $T = f(t)$ curves are shown in Fig. 4. This information is analogous to the thermocouple data that would normally be obtained experimentally. It is considered here as an "exact" result and used as the input data of the inverse task to study the response of the method.

The first test concerns the influence of a space step variation in the inverse region (Δr_2). For that test, Δt is constant (0.01 s), and we calculate the surface temperature and heat flux for several Δr_2 values (1/7, 1/11, 1/13, and 1/17 mm). The results, shown in Fig. 5, reveal that the accuracy of the calculation is seriously affected when Δr_2 is either too high or too low and the oscillations are not sensitive to Δr_2 variation. The deviation between direct and inverse results can exceed 10% in temperature and 30% in heat flux for $\Delta r_2 = 1/17$ mm.

At the heating/cooling transition, the computation results cannot account for the rapid change of the heat transfer. This can be attributed to the effect of the initial temperature radial profile used for cooling, which is nonuniform at the end of the heating procedure. This problem has already been studied for a steel quenching application (Ref 5). Excepting this instantaneous transition, a satisfying solution is obtained for $\Delta r_2 = 1/11$

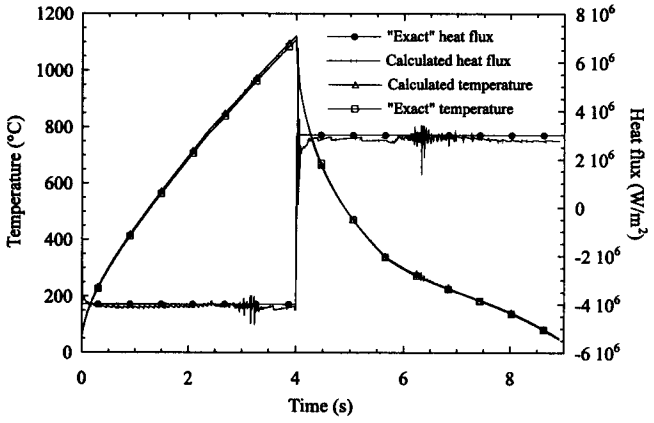

Fig. 7 Optimized surface temperature and heat flux evolutions (martensitic transformation)

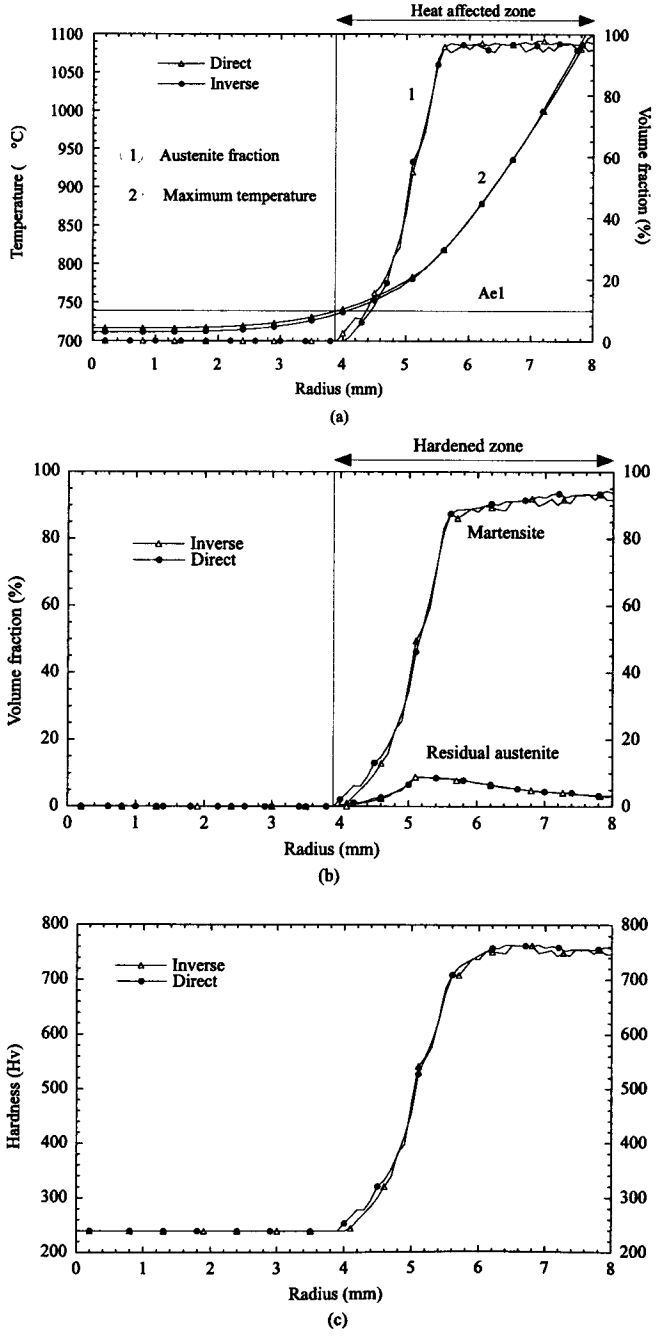

Fig. 8 XC42 steel. (a) Austenite and temperature profiles at the end of heating. (b) Martensite and retained austenite at the end of cooling. (c) Hardness profile

mm (11 points are considered in the inverse region) where the temperature difference does not exceed 4% and the heat flux difference does not exceed 10%.

The second test concerns the influence of a time step variation. In that case, Δr_2 is constant (1/11 mm), and we calculate the surface temperature and heat flux for several Δt values (0.05, 0.01, and 0.005 s). It should be noted (Fig. 6) that the estimated heat flux oscillates around the "exact" solution and the amplitude of the oscillations increases when Δt is too small, especially in the phase transformation domains. This can be filtered by increasing Δt without significantly affecting the solution.

These tests show that the precision of the inverse method is conditioned by the space step and that the stability is closely related to the time step. Then, in order to obtain a realistic estimation, it is necessary to compromise between stability and precision by finding an adequate choice of the Δt and Δr_2 steps.

3.3 *Application Examples*

3.3.1 XC42 Steel

In this application, we use the temperature evolution shown in Fig. 4 for an XC42 steel cylinder. This condition imposed at the specimen boundary (high heating and cooling rate) has been chosen in order to promote austenitization and subsequent martensitic transformation in the superficial zone (surface-hardening heat treatment). The inverse calculations are performed using the optimum values of space and time steps (Δt = 0.01 s and Δr_2 = 1/11 mm). The corresponding thermal results are reported in Fig. 7. The oscillations in the heat flux evolution are mainly due to the numerical convergence in the austenitic and martensitic transformation domains. Globally, this computational model gives very precise surface temperature and heat flux evolutions in both heating and cooling treatments.

Taking a metallurgical point of view, the radial profile of the maximum temperature reached on heating and the austenite volume fraction are computed. They are reported in Fig. 8(a). It is evident that the austenite fraction in the inner region (r = 0.0 mm, r = 3.8 mm) is null due to an insufficient temperature at the end of heating, which is lower than the transformation temperature (Ac_1 = 740 °C). The superficial zone (r = 5.4 mm, r = 8 mm) is completely austenitized. Using the inverse method, the austenite volume fraction reached at the end of heating is in very good agreement with the direct method calculation results.

On cooling, the martensite fractions and hardness level evolutions are calculated. The radial profile, at the end of cooling, of the martensite and retained austenite fraction is shown in Fig. 8(b) and that of the hardness is shown in Fig. 8(c). They re-

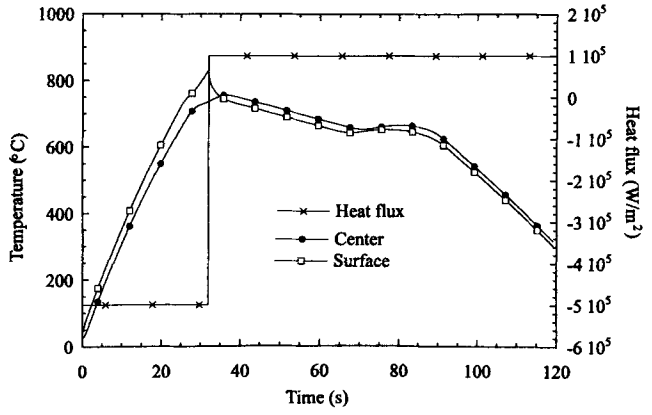

Fig. 9 Direct calculation: input exact heat flux and calculated temperature evolutions (XC80 steel)

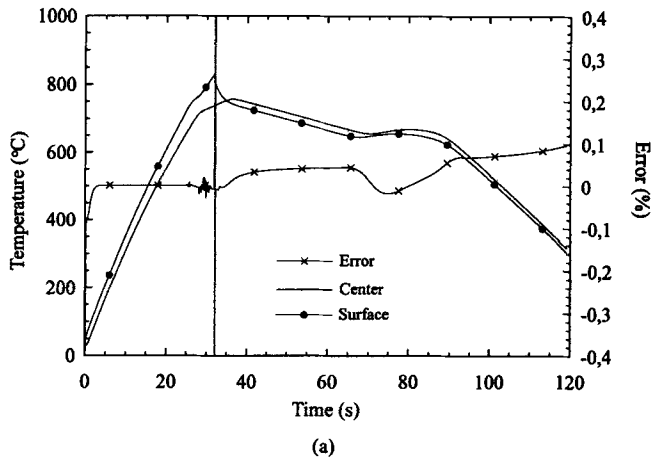

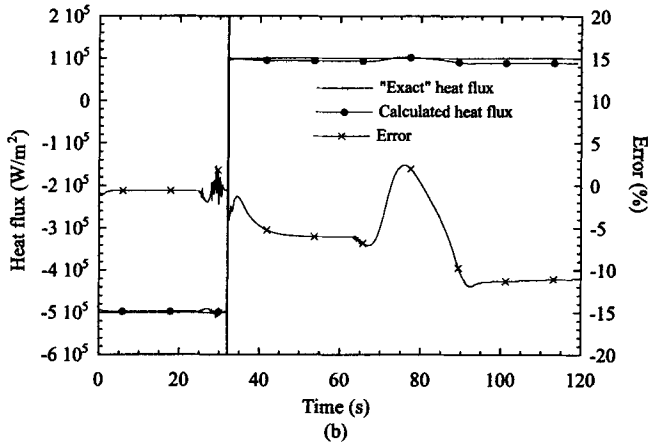

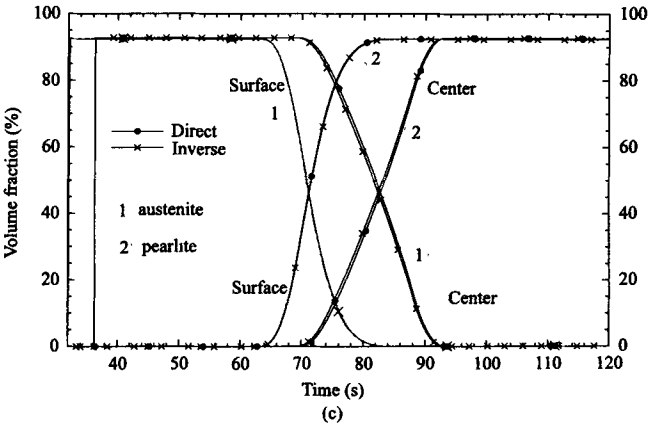

Fig. 10 Inverse calculation. (a) Temperature and error evolutions. (b) Heat flux and error evolutions. (c) Austenite and pearlite evolutions versus time

veal the expected surface hardening and are consistent with those obtained with the direct calculations.

3.3.2 XC80 Steel

Consider an XC80 steel (eutectoid steel) cylinder. The heat flux evolution imposed at the surface of the cylinder to generate the temperature evolution at inner position $r = r_e$ (1 mm under the active surface) is shown in Fig. 9. This heat flux evolution (low cooling rate) is especially chosen to promote pearlitic transformation, generating a consequent internal energy.

The inverse calculations are performed with $\Delta r_2 = 1/10$ mm and $\Delta t = 0.01$ s. The calculated temperature, heat flux, and austenite-pearlite volume fraction evolutions are presented in Fig. 10. On cooling, the temperature increase due to austenite-pearlite transformation is observed. The temperature and heat flux predictions are very correct if one compares the inverse and the direct calculations. The deviation does not exceed 0.1 and 10%, respectively. Compared to the previous case, this improvement is mainly due to the low heating and cooling rates, leading to a low thermal gradient at the end of heating and during pearlitic transformation.

5. Conclusions

In this study a numerical model of the inverse heat conduction problem taking into account the phase transformations has been developed to predict the thermal evolution (surface temperature, heat flux) and to estimate the phase transformation during heating and cooling of cylindrical specimens. We have studied the calculation sensitivity to space and time step variations. We can conclude that precision is conditioned by Δr_2 and that stability is closely related to Δt. We also have tested the phase transformation calculation and shown that the inverse method gives satisfying results in both thermal and transformation kinetics.

This work is continuing in order to establish the tolerable limits of this inverse method. Particular attention is being paid to (1) the sensitivity of the calculations, (2) the error measurements, (3) the thermocouple locations, and (4) the thermophysical properties of the material.

References

1. J.V. Beck, B. Litkouhi, and St. Clair, Efficient Sequential Solution of the Nonlinear Inverse Heat Conduction Problem, *Numer. Heat Transfer,* Vol 5, 1982, p 275-286
2. J.R. Burggraf, An Exact Solution of the Inverse Problem in Heat Conduction, Theory and Application, *J. Heat Transfer,* Vol 86, 1964, p 373-382
3. J.V. Beck, Surface Heat Flux Determination Using an Integral Method, *Nucl. Eng. Des.,* Vol 7, 1968, p 170-178
4. C.F. Weber, Analysis and Solution of the Ill-Posed Inverse Heat Conduction Problem, *Int. J. Heat Mass Transfer,* Vol 24, 1981, p 1783-1792
5. P. Archambault and A. Azim, Inverse Resolution of Heat Transfer Equation: Application to Steel and Aluminum Alloys Quenching, *J. Mater. Eng. Perform.,* Vol 4 (No. 6), 1995, p 730-736
6. S. Denis, D. Farias, and A. Simon, Mathematical Model Coupling Transformation and Temperature Evolutions in Steels, *ISIJ Int.,* Vol 32 (No. 3), 1992, p 316-325
7. Y. Dardel, *La transmission de la chaleur au cours de la solidification, du réchauffage et la trempe de l'acier,* Editions de la Revue de Métallurgie, Paris, 1964
8. F.M.B. Fernandes, C. Basso, S. Denis, and A. Simon, *Mater. Sci. Technol.,* Vol 1 (No. 10), 1985, p 838-844